ACSNANO
www.acsnano.org
ARTICLE

Extreme Light Management in Mesoporous Wood Cellulose Paper for Optoelectronics

Hongli Zhu,[†,⊥] Zhiqiang Fang,[†,⊥] Zhu Wang,[‡] Jiaqi Dai,[†] Yonggang Yao,[†] Fei Shen,[†] Colin Preston,[†] Wenxin Wu,[§] Peng Peng,[§] Nathaniel Jang,[†] Qingkai Yu,[∥] Zongfu Yu,[‡] and Liangbing Hu*[,†]

[†]Department of Materials Science and Engineering, University of Maryland, College Park, Maryland 20742, United States
[‡]Electrical and Computer Engineering, College of Engineering, University of Wisconsin—Madison, Madison, Wisconsin 53706, United States
[§]2D Carbon (Changzhou) Tech Company, Ltd., and Jiangnan Graphene Institute, Changzhou, Jiangsu 213161, China
[∥]Ingram School of Engineering, and MSEC, Texas State University, San Marcos, Texas 78666, United States

Supporting Information

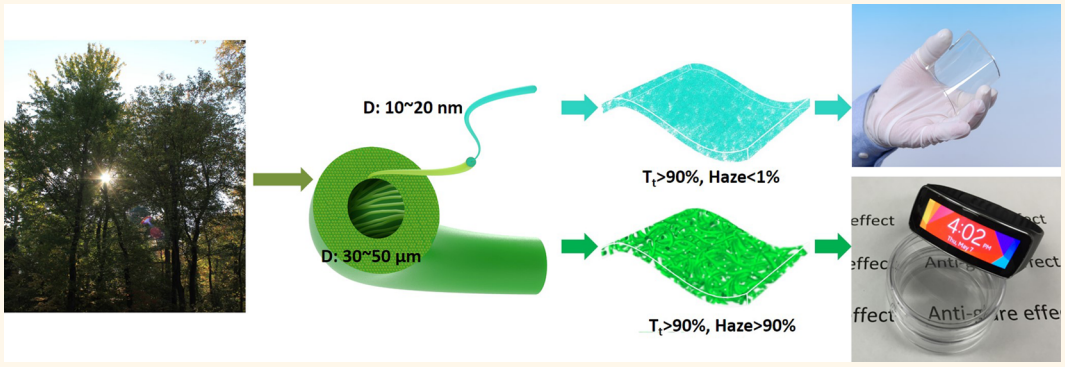

ABSTRACT: **Wood fibers possess natural unique hierarchical and mesoporous structures that enable a variety of new applications beyond their traditional use. We dramatically modulate the propagation of light through random network of wood fibers. A highly transparent and clear paper with transmittance >90% and haze <1.0% applicable for high-definition displays is achieved. By altering the morphology of the same wood fibers that form the paper, highly transparent and hazy paper targeted for other applications such as solar cell and antiglare coating with transmittance >90% and haze >90% is also achieved. A thorough investigation of the relation between the mesoporous structure and the optical properties in transparent paper was conducted, including full-spectrum optical simulations. We demonstrate commercially competitive multitouch touch screen with clear paper as a replacement for plastic substrates, which shows excellent process compatibility and comparable device performance for commercial applications. Transparent cellulose paper with tunable optical properties is an emerging photonic material that will realize a range of much improved flexible electronics, photonics, and optoelectronics.**

KEYWORDS: *wood cellulose materials, light management, high transparency, super clarity, super haze, paper touch screen, optoelectronics*

Transparent optical materials are one of the most important building blocks for optical devices.[1−5] These materials are used in a wide range of applications, ranging from windshields, lenses, and optical fibers to solar cells.[6−9] Silicon dioxide has long been the traditional material used for these applications due to extremely low absorption with super high transmittance. When SiO_2 is forged into crystal or glass, it is rigid at room temperature, which impedes the formation of new compelling flexible devices such as artificial skin, intelligent textiles, or flexible implants.[10−14] In the coming decades, flexible devices will be thoroughly developed with the integration of advanced electrical and optical functions. A high-performance transparent optical material that may replace SiO_2 and enable flexible optical devices or components is still lacking. This new transparent material ideally should exhibit low cost, low absorbance, high specular transmission, and compatibility with other materials. Plastic has been studied as a replacement for SiO_2 in flexible optical devices over the past decades, but plastic has intrinsic problems such as low thermal

Received: October 27, 2015
Accepted: December 16, 2015
Published: December 17, 2015

DOI: 10.1021/acsnano.5b06781
ACS Nano 2016, 10, 1369−1377

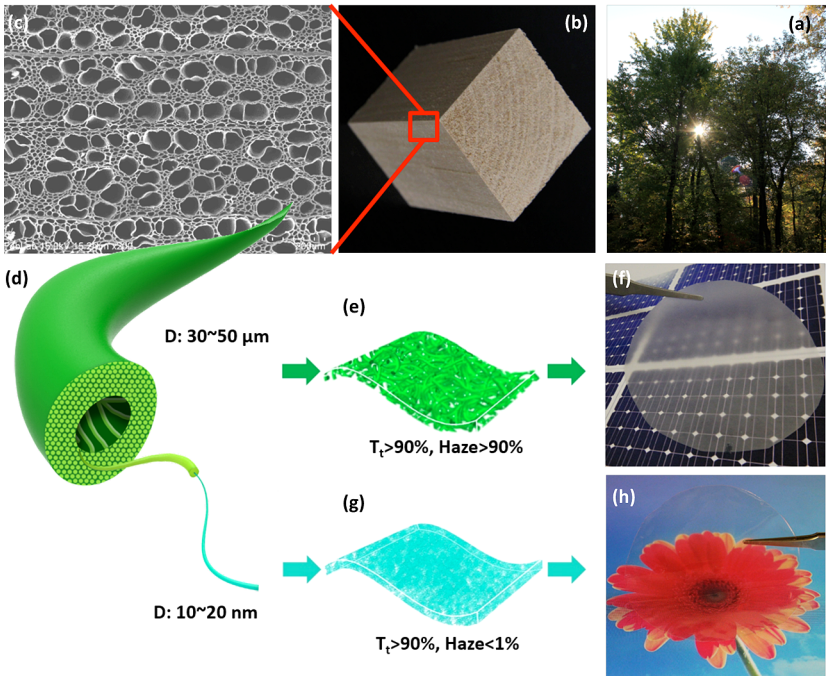

Figure 1. Hierarchical structure of tree and the applications of natural fibers with different fiber diameter. Images of (a) tree and (b) wood trunk. (c) SEM image of porous and fibrous structure of wood. (d) Hierarchical structure of wood microfiber, where each microfiber is composed of nanofibers. (e) Schematic and (f) picture of super transparent and super hazy paper made of partly dissolved and nanowelded microfibers. The total transmittance of hazy paper is >90%, and the transmission haze is >90%. (g) Schematic and (h) picture of super transparent and super clear paper made of nanofibers. The total transmittance of super clear paper is >90%, and the transmission haze is <1%.

stability, poor accessibility for functionalization, and harm to environment.[15−17]

Mesoporous materials are emerging toward novel photonics and optoelectronics, through which photons can be manipulated to achieve desired properties.[18] Note that, in this manuscript, mesopore is defined as a nanostructure that has hierarchical pore structures from micrometer size down to nanometer size. While traditional transparent substrates such as SiO_2 and plastic are solids, transparent paper is a mesoporous network of cellulose nanofiber (CNF) with controllable pore sizes and pore distributions.[19] This type of paper photonics has tremendous potential; the mesoporous structure of cellulose fiber-based paper allows the density, pore structure, and shape to be tuned dramatically, which is impossible to achieve with traditional plastic substrates.[20−29] It is expected, for example, that the mesopores can be filled with high index materials to create periodic photonic structures in paper. Mesoporous wood fiber-based paper can also be integrated in optofluidic devices due to the capacity to flow nanofluids through the transparent mesoporous structure. In the past few years, proof-of-concept devices such as transistors and solar cells have been demonstrated on transparent paper substrates.[24,30] Although these devices are completely functional, the optical properties do not adequately meet the desired standards. For example, the optical clarity is critical in displays that require a haze value (indication of optical scattering) less than 1%; however, the nanopaper demonstrated with cellulose nanofibers exhibits a haze value of around 10%, which is too high for high-definition displays.[31,32] A detailed understanding of the correlation between its structure and optical properties is still lacking.

In this work, we demonstrate that large light scattering tuning can be achieved in mesoporous paper for photonics and optoelectronics by simply changing the packing of the cellulose fibers. In one extreme, we achieved >90% total transmittance and <1% optical haze, when cellulose nanofibers are densely packed through layer by layer. In the other extreme, we achieved >90% total transmittance and >90% light scattering when the microfibers are *in situ* nanowelded in ionic liquid. We conducted a detailed investigation of the 3D surface topology of mesoporous cellulose paper. This 3D topology investigation supports a full spectrum simulation that may guide future designs of transparent paper with tunable light scattering. A 2.5 × 4 $in.^2$ touch screen (multitouch) is demonstrated using dry-transferred graphene as a transparent conductor on super clear paper. Mesoporous transparent paper with tailored optical properties can be applied to a range of devices resulting in an enhanced performance. Meanwhile, such super clear paper shows complete process compatibility with roll-to-roll manufacturing in flexible electronic, which is critical for future system integrations for all paper photonics and optoelectronics systems.

RESULTS AND DISCUSSION

Wood is a porous and fibrous structural tissue of trees (Figure 1a−c), consisting of microfibers with a hierarchical structure, as shown in Figure 1d. A large microfiber is composed of thousands of nanofibers.[33−35] In this work, we fabricate paper with high total forward transmittance but dramatic different light scattering behavior *via* two different strategies. The key design principle is that rich nanostructures with tailored mesopores allow us to control the scattering of photons through such random media. The collective behavior at the microscale leads to macroscopic optical properties.

To achieve different microstructures, we design and fabricate paper substrates using wood cellulose fibers with two different size dimensions. The resulting paper shows dramatically

DOI: 10.1021/acsnano.5b06781
ACS Nano 2016, 10, 1369−1377

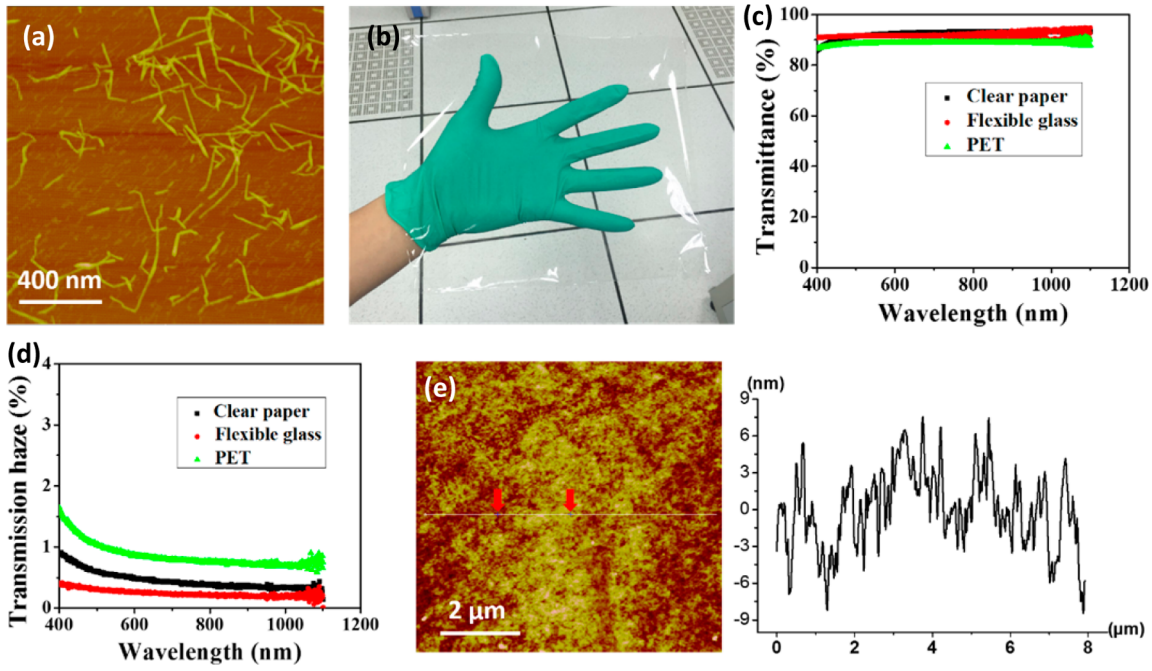

Figure 2. Super clear paper made of CNF exhibits excellent optical properties and small surface roughness. (a) AFM image of purified CNF with a uniform diameter. (b) Picture of super clear paper substrate. Comparison of total forward transmittance (c) and transmittance haze (d) for clear paper, flexible glass, and PET plastic. (e) AFM height image and AFM line scan of transparent clear paper with scan size of 8 × 8 μm^2.

different optical scattering behavior. In one case, the resulted paper is very hazy with significant amounts of mesopores and a relatively rougher surface than the clear paper (Figure 1e,f). The hazy paper is directly fabricated *via* nanowelding microfibers in ionic liquid. These welded microfibers lead to much denser packing than regular paper, which dismisses the large air cavities (~50 μm) and leads to the high optical transmittance. Meanwhile, a significant amount of mesopores still exist, which causes significant light scattering through the ~40−50 μm thick paper. In another case, the paper substrate is super clear with a small quantity of mesopores and a uniform surface texture (Figure 1g,h). The building block of the clear paper is a purified nanofiber disintegrated from wood fiber that exhibits a uniform size with diameter around 10−20 nm and a length around 500 nm. These nanofibers with excellent flexibility lead to a dense microstructure and optical appearance is as clear as high-quality SiO_2 glass. We significantly manipulate the light scattering in highly transparent paper by tailoring the fiber dimensions and packing density; the collective result is that the optical haze is adjustable between smaller than 1% and larger than 90% with transmittance larger than 90%.

Following the design in Figure 1g, we achieved optically clear paper with the lowest haze that has not been reported in literature. The detailed procedure for its fabrication is discussed in the Materials and Methods and Supporting Information (Figure S1a−d). To summarize, the CNF (Figure 2a) was obtained by a homogenization of 2,2,6,6-tetramethylpiperidine-1-oxyl (TEMPO)-oxidized wood fibers and then a centrifugation to remove any residual microfibers. The TEMPO treatment was used to swell the cell wall of the wood fibers. A uniform CNF with a diameter of ~20 nm was obtained after further homogenization and centrifugation treatment. The clear paper in size A4 as shown in Figure 2b was prepared through a scalable casting method with this uniform CNF suspension.

We further investigate the total transmittance and the transmittance haze of optically clear paper using a UV−vis spectrometer with an integrating sphere. The total transmittance is ~90% from wavelengths 400−1100 nm, which is similar to thin flexible glass (Corning, Inc., USA) and polyethylene terephthalate (PET). The optical haze of clear paper is 0.5% at 550 nm, which is similar to a glass substrate. This value meets the standards for high-end displays, which require an optical haze value less than 1%.[36−38] Our clear paper made of purified CNF shows a much smaller haze value than previous reported nanopaper.[31] Approximately 5% by weight of microfibers were removed during centrifugation at CNF purification step. Surprisingly, the transmittance haze decreases dramatically from 10% for nanopaper with noncentrifuged CNF to 0.5% for clear paper when such low amount of microfibers were removed (Figure S3). The mechanisms of optically clear paper with CNF fibers that may explain this behavior include: (1) the nanosized CNF building blocks scatter light much less than larger fibers (*i.e.* microfibers);[31,39] (2) the uniform CNFs and strong fiber−fiber interactions during the drying process lead to excellent packing toward a dense structure (density 1.2 g/cm^3), which decreases the light scattering through the bulk paper; (3) clear paper shows a super smooth surface (root-mean-square roughness ~2.6 nm, as discussed below) that induces negligible light scattering at the surface. The angular distribution of transmitted light was measured with a rotating light detector (Figure S4) and the normal direction of transmitted light was defined as 90°. All (100%) light is concentrated at 90° ± 1°, with the presence of 0.5% transmittance haze (Figure S5). The transmitted light is concentrated on the incident direction with no scattering.

Clear paper made of one-dimensional CNFs exhibits excellent mechanical strength and a smooth surface roughness. Compared to plastic that is made of homogeneous polymer, the clear paper is composed with one-dimensional nanofibers that

DOI: 10.1021/acsnano.5b06781
ACS Nano 2016, 10, 1369−1377

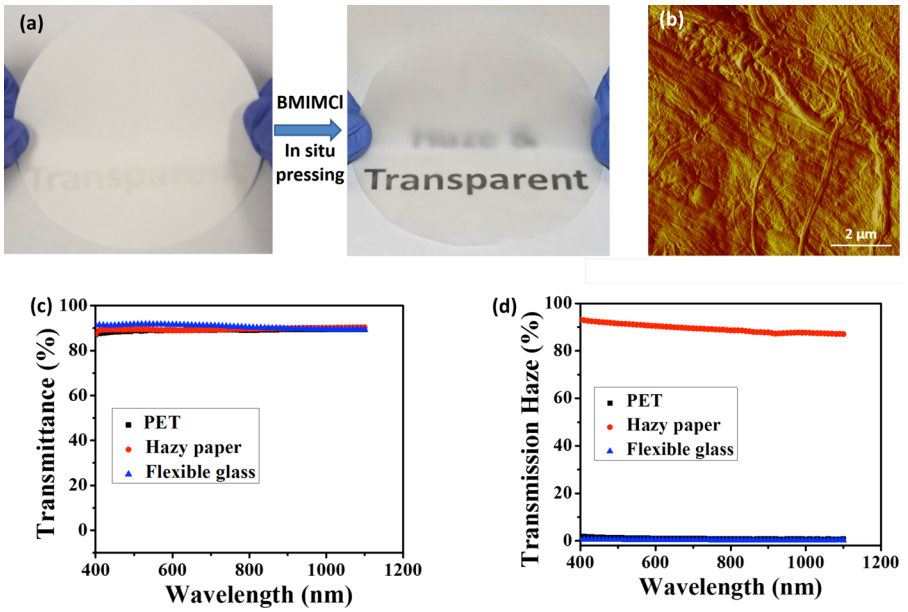

Figure 3. Super hazy paper fabricated by nanowelding exhibits excellent optical properties and surface roughness. (a) *In situ* pressing the ionic liquid treated paper turns a regular paper into a highly transparent and hazy paper. (b) AFM phase image with a size of 8 × 8 μm^2 showing the surface morphology of super hazy paper. Comparison of total forward transmittance (c) and transmittance haze (d) for super hazy paper, flexible glass, and PET.

possess rich hydroxyl groups. Coupled with the outstanding mechanical properties of individual CNFs (Young's Modulus 150 GPa of cellulose nanocrystal),[40,41] the network structure linked by strong hydrogen bonds between CNFs leads to both excellent mechanical strength and flexibility in clear paper (Figure S6a,b). Surprisingly, the mesoporous clear paper with a network structure has a small surface roughness, as shown in Figure 2e. The atomic force microscope (AFM) topographical line scan reveals root-mean-square (RMS) roughness of 2.6 nm.

We also invented a simple and fast *in situ* pressing method with partially dissolved microfibers to fabricate super hazy paper. The detailed procedure is presented in Materials and Methods. To summarize, a piece of paper made with regular microfiber was immersed in ionic liquid 1-butyl-3-methylimidazolium chloride (BMIMCl) for 15 min. The paper saturated with ionic liquid was then *in situ* hot-pressed. The ionic liquid breaks down the hydro bonds between the cellulose chains and effectively dissolves the surface layer of the fibers while retaining the microfiber backbones.[42−44] Additional washing in methanol was used to remove ionic liquid inside the hazy paper. The paper changes from opaque to transparent after the ionic liquid treatment (Figure 3a). The *in situ* dissolution of microfibers under hot-pressing serves two purposes: (1) the dissolved surface leads to strong nanowelding between microfibers; (2) the microsized vacancies initially occupied by air in the paper are filled by dissolved cellulose under pressure. The dissolved cellulose nanofibers by ionic liquid during *in situ* pressing are clearly observable in the finished paper (Figure 3b). The *in situ* pressing greatly increases the packing density and removes the microsized cavities filled with air in the paper, which leads to the high transmittance. Note that the density of initial paper is 0.5 g/cm^3, while the density of hazy paper is ~1.1 g/cm^3.

We characterized the optical properties of transparent and hazy paper with an integrating sphere and a rotating light detector. The *in situ* pressed paper shows a high optical transmittance of up to 90% at 550 nm, which is comparable to flexible glass and PET (Figure 3c). Interestingly, the transparent paper also shows a super high haze value for forward transmitted light, with a value of 91% at 550 nm (Figure 3d). Note that the transmittance haze for glass and PET is less than 1%.[45,46]

Both the hazy paper and the clear paper are fabricated with essentially the same material of wood cellulose fibers. The unique combination of high transmittance and high haze results from the unique structure. The porous structure in the paper causes numerous light scattering, which randomly redirects light's propagation path and leads to the high haze in the transmission. The strength of the scattering sensitively depends on the size of the pores. Clear paper has mesopores on the scale of a few nanometers, much smaller than the optical wavelength, which has a minimal scattering angle. In contrast, hazy papers have additional pores hundreds of nanometers in size, leading to much larger light scattering angles.

We have demonstrated that a dramatically different light scattering behavior is achieved in highly transparent paper. Since the essential material for both paper substrates is the same, cellulose, the dramatic difference in the optical properties results from their structures. To correlate the optical properties with the structure of two different types of paper, we investigate the pore distributions of the substrates with various different techniques resolute to different length scales. Brunauer−Emmett−Teller (BET) measurement was carried out to characterize pores with a diameter less than 100 nm (Figure 4a). Both types of paper possess mesopores with a peak at the same pore size of 4 nm. Although the pores are similar in both paper substrates, hazy paper has about twice the pore volume than the clear paper. We used a magnified AFM with a scan area of 1 × 1 μm^2 to further obtain the pore size and size distribution for two kinds of paper (Figure 4c,d). Clear paper shows a much denser surface containing mesopores in the range of 10−20 nm, which agrees with the BET measurement. Similar AFM images at different spots were taken, which did not show pores with a size larger than the 100 nm exhibited in

DOI: 10.1021/acsnano.5b06781
ACS Nano 2016, 10, 1369−1377

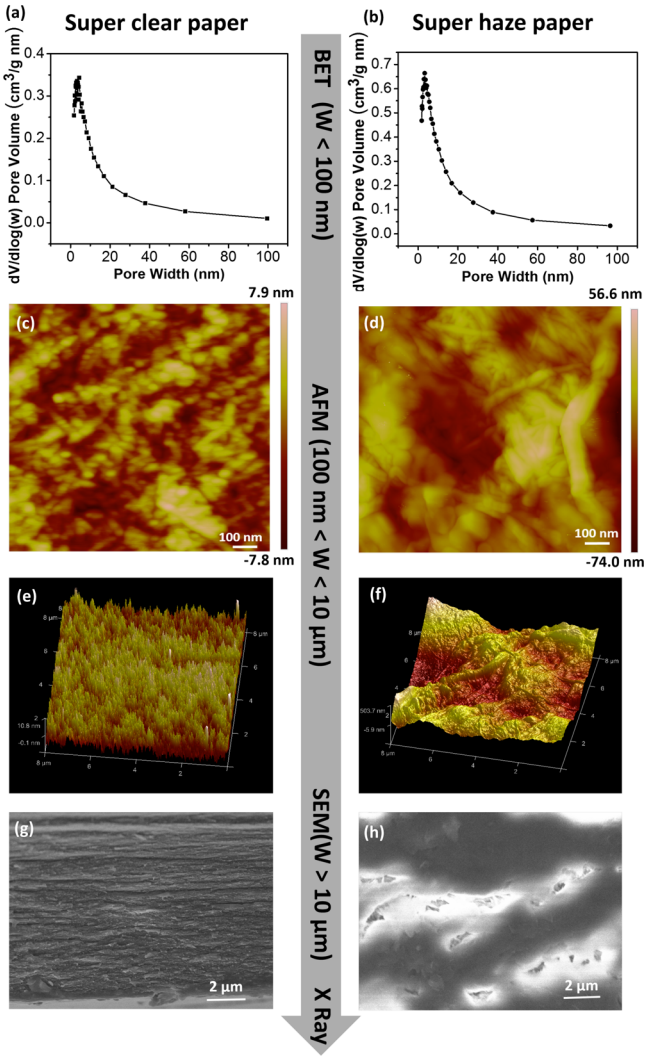

Figure 4. Characterizations of mesoporous structures in clear and hazy paper at different length scales. BET-BJH pore distributions, AFM height images (scan area, 1 × 1 μm^2), 3D AFM images (scan area, 8 × 8 μm^2), and cross-sectional SEM image for clear paper are shown in (a), (c), (e), and (g), respectively. The same characterizations are shown for hazy paper in (b), (d), (f), and (h).

clear paper. However, hazy paper possesses pores with a size close to 0.5 μm.

Since the AFM image with a 1 × 1 μm^2 scan area only reveals the local structure of paper, a 3D AFM with a much larger scan area (8 × 8 μm^2) was used to investigate surface roughness and 3D morphology (Figure 4e,f) of two papers with the same thickness (40−50 μm). The hazy paper shows a much rougher morphology than the clear paper. The peak−valley height difference is 9.3 nm in the clear paper and 488 nm in the hazy paper. More AFM data that reveals the surface morphology is found in Supporting Information (Figures S7 and S8). Cross-sectional scan electron microscope (SEM) by breaking the sample in liquid nitrogen reveals pores with a size of 1−2 μm for hazy paper. Statistics counting reveals there are ∼3% volume pores in this size range. No pores in this range were observed in SEM images of clear paper, Figure 4g,h. We used X-ray topography to investigate pores larger than 10 μm in hazy paper (Video 1 can be found in the Supporting Information). The microfiber backbone and the layer-by-layer structure are well-defined in the hazy paper (Figure S9a,b). The BET-BJH data shows that the regular fibers also possess mesopores (Figure S10a), but the pore between the neighboring fibers is mostly at ∼50 μm (Figure S10b). Note that both the clear and the hazy paper show a much higher packing density than the regular paper (Figure 4g,h and Figure S10). The four different measurements, BET, AFM, SEM, and X-ray topography, at different length scales reveal dramatically structural difference between clear paper and hazy paper. Due to the fibrous structure, clear paper has a mesoporous structure that is not seen in traditional transparent substrate (*i.e.*, glass or PET). Hazy paper contains additional pores with a larger size (∼0.5−1 μm), but lacks pores seen in regular paper (∼50 μm or larger). Pores with a size ∼0.5−1 μm are close to the wavelength of visible light, which causes the prominent light scattering that causes a high haze value.

The transmission haze is caused by the scattering of light through the paper, which is closely connected to its microscopic structure. To study this connection in our mesoporous paper, we performed full-wave optical simulations to characterize the light scattering based on the mesostructure measured by a 3D AFM. The AFM measurements in Figure 4 show that the spatial variation across the surface is significantly greater in the hazy paper than in the clear paper. The RMS of the surface height of the hazy paper is 137 nm, on the same order of magnitude as the visible light wavelength. In contrast, the RMS for the clear paper is only 2.6 nm. The refractive index of the cylinders is 1.5 and the height is 200 nm for the hazy paper (Figure 5a). We tune the distribution of the radius and positions of the cylinders so that the RMS of the surface height is the same as the hazy paper. Similarly, smaller cylinders are used to model the surface morphology of the clear paper as shown in Figure 5b. The height is 5 nm to keep the RMS the same as the clear paper. We use Stanford Stratified Structure Solver (S4) to solve the Maxwell's equations in the frequency-domain.[47] Periodic boundary conditions are used with a period of 8 μm in the lateral directions. Since the period is much larger than the wavelengths of visible light, we expect to see a large number of diffraction beams when light passes through the structure. The light intensity in these diffraction directions directly measures the strength of light scattering. To visualize the scattering strength, we show the intensity in all forward-diffracted directions. These directions are labeled by their parallel wave vectors:

$$(k_x, k_y) = (m, n)\frac{2\pi}{a} \tag{1}$$

Where integers 'm, n' are the order number; a = 8 μm is the period. The wave vector in the vertical direction is calculated as

$$k_z = \sqrt{\left(\frac{2\pi}{\lambda}\right)^2 - k_x^2 - k_y^2} \tag{2}$$

Where λ is the wavelength (500 nm). The direction of the wave vector determines the propagation direction of the scattered light. As shown by Figure 5c,d, light passing through the surface with a large spatial variation (Figure 5a) is redistributed to a wide range of different diffraction directions (Figure 5c). In contrast, there is almost little light scattering (Figure 5d) for the case of the surface with a small spatial variation (Figure 5b). The direct forward transmission in the normal direction is intentionally neglected in order to better visualize the scattered light.

DOI: 10.1021/acsnano.5b06781
ACS Nano 2016, 10, 1369−1377

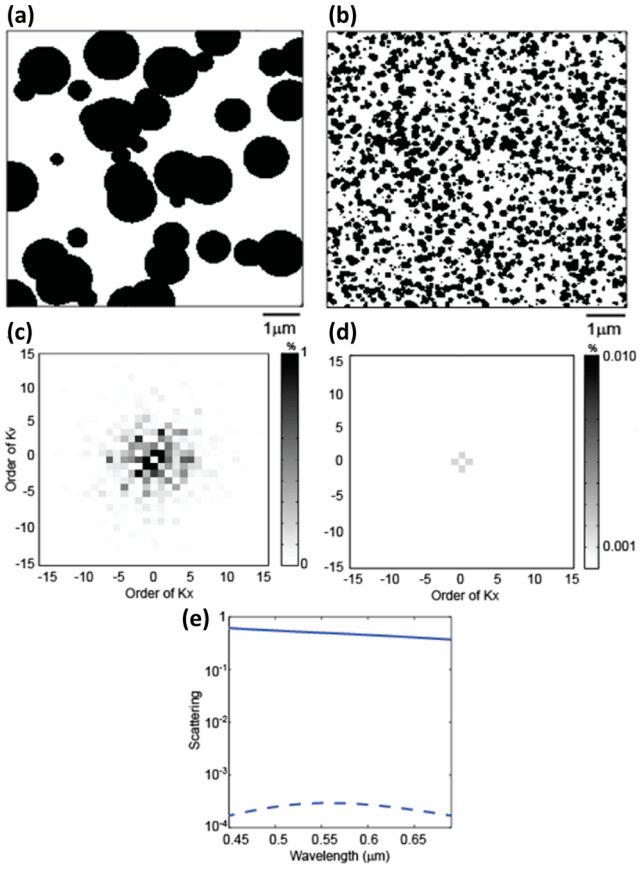

Figure 5. Optical simulation of light scattering of super hazy paper and super clear paper. Top view of the structures used for the modeling of the hazy (a) and the clear (b) papers, respectively. The black represents a material with refractive index n = 1.5, while the white represents empty space. The heights are 200 and 5 nm for (a) and (b), respectively. The structure of (a) is placed on a 200 nm thick uniform material (n = 1.5). (c and d) The distribution of scattered light when a normally incident light passes through the structure (a) and (b), respectively. Data is shown in percentage of incident light energy. (e) The spectra of scattered light for hazy paper (solid line) and clear paper (dashed line) in visible wavelength range.

We further show the scattering of light over the entire visible wavelength range for these two different paper models. Figure 5e shows the amount of the light scattered by the structures, *i.e.*, transmission haze, in Figure 5a,b assuming light is incident at the normal direction. It can be clearly seen that the surface with large spatial variation (Figure 5a) scatters light strongly (solid line Figure 5e), causing the paper to appear hazy. On the other hand, the surface with small spatial variation surface (Figure 5b) has extremely weak light scattering and causes the high clarity of the paper.

Paper with a large forward transmittance and controllable scattering (being high clarity or high haze) can be used for a range of emerging photonics and optoelectronics. For example, super hazy transparent paper has a large angular distribution of light scattering that can be used in optoelectronics such as solar cells and thin-film organic light-emitting diodes, where coupling of light into or out of the devices is crucial for high performance devices. Super clear paper has a similar clarity as high display-quality glass and plastics. As opposed to glass and plastic, clear paper is mesoporous with simultaneous nanometer scale smoothness. The 3D mesoporous structure in clear paper can enable new bulk engineering routes by loading nanometer sized molecules or flowing nanofluidic toward 3D photonic or 3D fluidic.

Super clear paper developed here has an optical haze as low as plastic substrates that is extremely promising for a range of future optoelectronics. To prove that super clear paper is compatible with the processing for commercial devices, we demonstrated the first high-performance capacitive paper touch screens using the processes and designs for the commercial plastic-based touch screen. Figure 6a illustrates the structure of

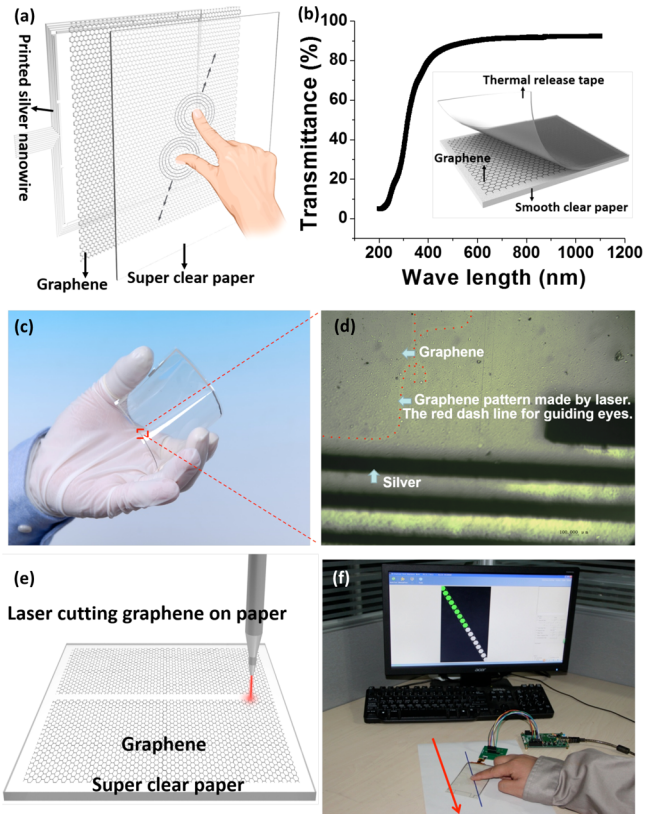

Figure 6. Super clear paper based multitouch screen with a thin layer of graphene as a conducting electrode. (a) A schematic of paper based multitouch screen. (b) Optical transmittance of whole device. The inserted schematic shows the dry transferring process for graphene on clear paper. (c) Picture of a highly flexible, invisible paper touch screen. (d) The zoomed-in image to show detailed graphene electrodes and metal contacts patterned by laser. The red dash line is drawn for guiding eyes. (e) Schematic showing the procedure of laser cutting graphene on paper. (f) Measurement of linearity of paper touch screen.

a capacitive-based multipoints touch screen. The patterned graphene layer is used as a group of electrodes and the mutual capacitance of those electrodes is monitored by a designed circuit. The human fingers function as the other electrode to form the local capacitor. Local capacitance upon touch can introduce an electrical signal to identify touch position. Compared to a resistive touch screen, the capacitive touch screen has the advantage of higher sensitivity, longer life, and response to the multipoints touch. As shown in the inserted image of Figure 6b, chemical vapor deposited (CVD) single layer graphene was dry-transferred onto a piece of clear paper as a replacement for conventional indium tin oxide (ITO) as a transparent electrode. The smooth surface of the clear paper

DOI: 10.1021/acsnano.5b06781
ACS Nano 2016, 10, 1369–1377

leads to an excellent performance of the graphene-on-paper, with a sheet resistance of 445 Ohm/sq and transmittance of 89% in the visible range (Figure 6b). The dry-transferred graphene on paper has a similar performance to that of plastic, which confirms its compatibility for processes.[37]

A working paper touch screen device with a size of 2.5 × 4 in.^{2} is demonstrated, which shows excellent flexibility and high clarity (Figure 6c). Detailed fabrications processes can be found in the Materials and Methods. A metallic film with the thickness 8 μm was printed at the edges of the defined area of graphene electrodes by screen-printing of silver paste. A laser beam was applied to sputter the metal frame into metal lines and cut the graphene area to form patterns (Figure 6d, Figure S11), where the red dotted lines guide the laser burning path. Any two adjacent burning traces define a graphene electrode, which is connected with an aforementioned metallic line patterned by a laser too. The laser is a solid state fiber laser with a wavelength of 1064 nm. We used a 2 W laser power for patterning graphene which schematically shows in Figure 6e and 8 W for patterning silver contacts. The integrated driving circuit is bonded with metal contacts on paper at the end of the module. Clear paper shows excellent compatibility with various device fabrication processes that are optimized for plastic dry-transfer, screen printing, laser cutting, and metal contact integrations.

Figure 6f shows our test on the linearity, an important parameter to reflect the performance of a touch screen. For a qualified touch screen, when a human's finger moves along a straight line, the device incorporated with the touch screen should respond to the exact locations where the finger passes. In the picture, the blue line drawn on paper under the touch screen was used for guiding the movement of a finger (a red arrow highlights the direction of the movement of a finger) and the image on the computer screen shows the response of the touch screen embedded in a testing module. The green dot on screen indicates the line section, where a finger has passed. The graphene-on-paper based touch screen has as excellent linearity as a high-quality commercial touch product. The mechanical durability test by bending shows no degradation of graphene quality after 10 000 times, which is more durable than the ITO on plastic (Figure S12). The as-fabricated touch screen is very flexible and its sensing performance is comparable to a regular commercial touch screen, Video 2 and Supporting Information Figure S13). The demonstrated capacitive graphene-on-paper touch screen can be used for emerging flexible display and touch module, which is urgently demanded in custom electronics but cannot be achieved by current touch screen technology based on ITO on plastics. While clear paper-based touch screens is as durable as its plastic counterpart, the entire device can be dissolved in water if required (Video 2 in Supporting Information). This is extremely attractive for consumer electronics, as the large demand worldwide is posing a great environment concern.

While super clear paper is extremely promising for high-resolution displays and optoelectronics, super hazy and transparent paper can offer an extremely effective light coupling when forward light scattering is preferred. The distribution of transmitted light through the super hazy paper was measured (Figure 7a), where 90° is the normal direction to the paper substrate. Note that most of the light is scattered away from the normal direction. The highly transparent and meanwhile hazy paper can effective couple light in or out for optoelectronics devices, such as solar cells and organic light emitting diode (OLED). As shown in Figure 7b, the emitted light in OLED

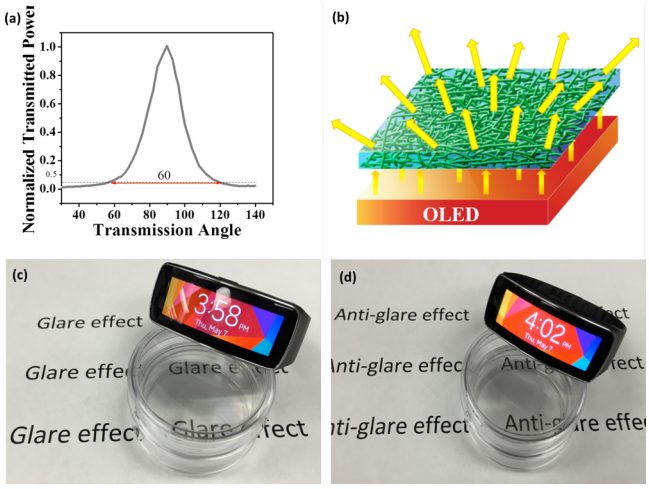

Figure 7. Light scattering and coupling in optoelectronics of super hazy paper. (a) Angular distribution of forward light scattering in transparent and super hazy paper; (b) enhanced light output by transparent and hazy paper in OLED device; (c and d) OLED display with and without super hazy paper coating, respectively, where hazy paper removes the glare effect.

device can be coupled out more effectively due to the antireflection effect of the hazy paper, which can, in turn, potentially increase the lighting efficiency. Similar advantage is expected for outdoor displays where glaring is always a problem due to the brightness of the ambient environment. Figure 7c,d shows that simply laminating a transparent and hazy paper on the OLED watch can effectively remove the glare effect.

CONCLUSION

In conclusion, this study provides the demonstration that precise control of the cellulose fiber dimensions enables paper substrates with a diverse range of unique optical properties. We experimentally and computationally investigate the relation between the mesoporous structure and its optical properties, and conclude that a three-dimensional network of cellulose fibers exhibit optical properties directly related to the fiber size. A network of smaller fibers forms a near perfectly clear transparent paper with haze <1.0%, while a network of larger fibers forms an entirely hazy transparent paper with haze >90%. A 2.5 × 4 in.^{2} multitouch touch screen was fabricated with graphene transferred on super clear paper, which demonstrates excellent process compatibility of transparent paper toward device integrations. Effective light coupling and antiglare effect was also demonstrated for super hazy paper in OLED lighting. Mesoporous transparent substrates made of wood cellulose fibers will enable a new era of paper photonics, electronics, and optoelectronics that are not possible on other transparent substrates.

MATERIALS AND METHODS

Fabrication of Super Clear Paper. An aqueous TEMPO oxidation system first proposed by Isogai and colleagues was utilized to pretreat the bleached softwood pulp,[48−52] and for details, readers can refer to our previous papers.[30,31] Briefly, 1.0 wt % TEMPO-oxidized wood pulp was passed twice through thin z-shaped chambers with channel dimension of 200 μm in a Microfluidizer processor under a process pressure of 25 000 psi (M110 EH, Microfluidics, Inc., USA). The obtained CNF was diluted to 0.2 wt % with distilled water and kept stirring by a magnetic stirrer for 2 h to ensure the complete dispersion of CNF. Afterward, diluted CNF suspension was

DOI: 10.1021/acsnano.5b06781
ACS Nano 2016, 10, 1369−1377

centrifuged at the speed of 3000 rpm/min for 20 min to remove large cellulose bundles. The supernatant was transferred into a bottle *via* pipet. The purified CNF suspension was poured into a nonstick container and dried in a controlled chamber.

Fabrication of Super Hazy Paper. A regular paper with a thickness around 90 μm was fabricated by a vacuum filtration method with a well-dispersed suspension of southern yellow pine fiber. The dried sheet was immersed in BMIMCl ionic liquid at 90 °C for 15 min and then transferred to a hot-press for an additional 1 h treatment. After that, the sample was immersed in methanol (Sigma-Aldrich, USA) for 8 h to remove ionic liquid residue. After a rinsing step, the paper sheet was cold pressed and dried. The final paper has thickness of ~40 μm.

Fabrication of Touch Screen Graphene-on-Clear Paper. The fabrication process of the super clear paper/graphene touch screen is described below: (1) Graphene was grown on a Cu foil by CVD using methane as a precursor at 1030 °C. (2) For transferring graphene to super clear paper, thermal release tape was applied on the front side of graphene/Cu structure first, then oxygen plasma was used to etch the graphene at the back side of graphene/Cu structure, followed by dissolving the Cu foil in $Fe(NO_3)_3$. The thermal release tape/graphene structure was then laid on a super clear paper and heated at 100 °C to release the graphene from the thermal release tape onto the super clear paper, as illustrated in the inset image in Figure 6b. (3) The bilayer structure of graphene/clear paper was used to fabricate capacitive touch screens, where the graphene film was patterned as a group of electrodes.

Characterization. The optical properties of the paper were measured using a UV−vis Spectrometer Lambda 35 containing an integrating sphere (PerkInElmer, USA) based on standard ASTM1003-92 "Standard Method for Haze and Luminous Transmittance of Transparent Plastic". Surface characterization was performed using a Veeco multimode scanning probe microscope (SPM) with NanoScope V controller with a model SNL-10 silicon-on-nitride tip (Veeco) using a drive frequency of ~75 kHz and a spring constant of 0.58 N/m. Prior to imaging, paper samples were mounted on magnetic sample disks using double-sided tap. Scans were collected over areas ranging from 500 nm^2 to 8 μm^2 at a scan rates of 0.46−0.92 Hz. Image data were processed by planar background subtraction using Nanoscope Analysis software, version 1.4 (Bruker). Partially dissolved paper was characterized with a Hitachi SU-70 FESEM field effect scanning electron microscopy (SEM), performed using a Jeol JXA 840A system (Jeol Instruments, Tokyo, Japan) running at 5−10 keV. The paper surface area was measured with a Micromeritics TriStar II 3020 Porosimeter Test Station. The paper pore distribution was measured with a Micromeritics TriStar II 3020 Porosimeter Test Station. The range of measurable pore sizes is between 1.7 and 120 nm. The Barrett−Joyner−Halenda (BJH) adsorption average pore algorithm is used for evaluation. The hazy paper was tested in a Skyscan 1172 μCT for morphology analysis. The sample was scanned without a filter under 40 kV at 1.0 um pixels. The 3D images were reconstructed in NRecon. Touch screen performance was tested on TP Tool SIU board module operated by software FT Touch Studio.

ASSOCIATED CONTENT

Supporting Information

The Supporting Information is available free of charge on the ACS Publications website at DOI: 10.1021/acsnano.5b06781.

The procedures for preparing super clear paper, the AFM image of CNF for super clear paper, the transmission haze of super clear paper with/without purification of CNF suspension in the visible wavelength, schematic showing the measurement setup for angular dependent transmittance, angular distribution of forwarded light scattering of super clear paper, stress−strain curve of super clear paper and ultra hazy paper, X-ray topography of the super hazy paper, BET pore distribution and morphology of regular paper, laser patterning of graphene-on-paper, the durability and performance of super clear paper based touch screen (PDF)

Movie 1: X-ray topography (AVI)

Movie 2: Touch screen (AVI)

AUTHOR INFORMATION

Corresponding Author

*E-mail: binghu@umd.edu.

Author Contributions

⊥H.Z. and Z.F. contributed equally to this work.

Notes

The authors declare no competing financial interest.

ACKNOWLEDGMENTS

L. Hu acknowledges the support from the DOD (Air Force of Scientific Research) Young Investigator Program (FA95501310143). We acknowledge Peter Ciesielski in the National Bioenergy Center at National Renewable Energy Laboratory (Golden, CO) for helping us on the AFM images. Zhiqiang Fang would like to thank the China Scholarship Council (CSC) for their financial support.

REFERENCES

(1) Wu, H.; Kong, D. S.; Ruan, Z. C.; Hsu, P. C.; Wang, S.; Yu, Z. F.; Carney, T. J.; Hu, L. B.; Fan, S. H.; Cui, Y. A transparent electrode based on a metal nanotrough network. *Nat. Nanotechnol.* **2013**, *8*, 421−425.

(2) Ben-Sasson, A. J.; Tessler, N. Unraveling the physics of vertical organic field effect transistors through nanoscale engineering of a self-assembled transparent electrode. *Nano Lett.* **2012**, *12*, 4729−33.

(3) Xia, Y.; Sun, K.; Ouyang, J. Solution-processed metallic conducting polymer films as transparent electrode of optoelectronic devices. *Adv. Mater.* **2012**, *24*, 2436−2440.

(4) Hu, L. B.; Hecht, D. S.; Gruner, G. Carbon Nanotube Thin Films, Fabrication, Properties, and Applications. *Chem. Rev.* **2010**, *110*, 5790−5844.

(5) Zhang, C.; Zhao, D.; Gu, D.; Kim, H.; Ling, T.; Wu, Y. K.; Guo, L. J. An Ultrathin, Smooth, and Low-Loss Al-doped Ag Film and Its Application as A Transparent Electrode in Oganic Photovoltaics. *Adv. Mater.* **2014**, *26*, 5696−5701.

(6) Keiser, G. Optical Fiber Communications. *Wiley Encyclopedia of Telecommunications*; John Wiley & Sons, Inc., 2003.

(7) Wang, X.; Zhi, L.; Müllen, K. Transparent, Conductive Graphene Electrodes for Dye-Sensitized Solar Cells. *Nano Lett.* **2008**, *8*, 323−327.

(8) Wang, B.; Ye, M.; Sato, S. Lens of Electrically Controllable Focal Length Made by a Glass Lens and Liquid-Crystal Layers. *Appl. Opt.* **2004**, *43*, 3420−3425.

(9) Wu, J.; Becerril, H. A.; Bao, Z.; Liu, Z.; Chen, Y.; Peumans, P. Organic Solar Cells with Solution-processed Graphene Transparent Electrodes. *Appl. Phys. Lett.* **2008**, *92*, 263302.

(10) Someya, T.; Sekitani, T.; Iba, S.; Kato, Y.; Kawaguchi, H.; Sakurai, T. A Large-Area, Flexible Pressure Sensor Matrix with Organic Field-Effect Transistors for Artificial Skin Applications. *Proc. Natl. Acad. Sci. U. S. A.* **2004**, *101*, 9966−9970.

(11) Katragadda, R. B.; Xu, Y. A Novel Intelligent Textile Technology Based on Silicon Flexible Skins. *Sens. Actuators, A* **2008**, *143*, 169−174.

(12) Najafi, K.; Wise, K. D. An Implantable Multielectrode Array with On-Chip Signal Processing. *IEEE J. Solid-State Circuits* **1986**, *21*, 1035−1044.

(13) Kim, D. H.; Kim, Y. S.; Amsden, J.; Panilaitis, B.; Kaplan, D. L.; Omenetto, F. G.; Zakin, M. R.; Rogers, J. A. Silicon Electronics on Silk as A Path to Bioresorbable, Implantable Devices. *Appl. Phys. Lett.* **2009**, *95*, 133701.

DOI: 10.1021/acsnano.5b06781
ACS Nano 2016, 10, 1369−1377

(14) Berger, T. W.; Baudry, M.; Brinton, R. D.; Liaw, J. S.; Marmarelis, V. Z.; Yoondong Park, A.; Sheu, B. J.; Tanguay, A. R. Brain-Implantable Biomimetic Electronics as the Next Era in Neural Prosthetics. *Proc. IEEE* **2001**, *89*, 993−1012.
(15) McAlpine, M. C.; Ahmad, H.; Wang, D.; Heath, J. R. Highly Ordered Nanowire Arrays on Plastic Substrates for Ultrasensitive Flexible Chemical Sensors. *Nat. Mater.* **2007**, *6*, 379−384.
(16) Kim, D.-H.; Kim, Y.-S.; Wu, J.; Liu, Z.; Song, J.; Kim, H.-S.; Huang, Y. Y.; Hwang, K.-C.; Rogers, J. A. Ultrathin Silicon Circuits With Strain-Isolation Layers and Mesh Layouts for High-Performance Electronics on Fabric, Vinyl, Leather, and Paper. *Adv. Mater.* **2009**, *21*, 3703−3707.
(17) Mohanty, A. K.; Misra, M.; Drzal, L. T. Sustainable Bio-Composites from Renewable Resources, Opportunities and Challenges in the Green Materials World. *J. Polym. Environ.* **2002**, *10*, 19−26.
(18) Khan, M. K.; Giese, M.; Yu, M.; Kelly, J. A.; Hamad, W. Y.; MacLachlan, M. J. Flexible Mesoporous Photonic Resins with Tunable Chiral Nematic Structures. *Angew. Chem., Int. Ed.* **2013**, *52*, 8921−8924.
(19) Sehaqui, H.; Zhou, Q.; Ikkala, O.; Berglund, L. A. Strong and Tough Cellulose Nanopaper with High Specific Surface Area and Porosity. *Biomacromolecules* **2011**, *12*, 3638−3644.
(20) Yousefi, H.; Faezipour, M.; Nishino, T.; Shakeri, A.; Ebrahimi, G. All-Cellulose Composite and Nanocomposite Made from Partially Dissolved Micro-and Nanofibers of Canola Straw. *Polym. J.* **2011**, *43*, 559−564.
(21) Nishino, T.; Matsuda, I.; Hirao, K. All-Cellulose Composite. *Macromolecules* **2004**, *37*, 7683−7687.
(22) Horiuchi, N. Optical materials: Nanostructured Paper. *Nat. Photonics* **2014**, *8*, 172−172.
(23) Svagan, A. J.; Busko, D.; Avlasevich, Y.; Glasser, G.; Baluschev, S.; Landfester, K. Photon Energy Upconverting Nanopaper: A Bioinspired Oxygen Protection Strategy. *ACS Nano* **2014**, *8*, 8198−8207.
(24) Fang, Z.; Zhu, H.; Yuan, Y.; Ha, D.; Zhu, S.; Preston, C.; Chen, Q.; Li, Y.; Han, X.; Lee, S.; et al. Novel Nanostructured Paper with Ultrahigh Transparency and Ultrahigh Haze for Solar Cells. *Nano Lett.* **2014**, *14*, 765−773.
(25) Nakagaito, A. N.; Nogi, M.; Yano, H. Displays from Transparent Film of Natural Nanofibers. *MRS Bull.* **2010**, *35*, 214−218.
(26) Nogi, M.; Iwamoto, S.; Nakagaito, A. N.; Yano, H. Optically Transparent Nanofiber Paper. *Adv. Mater.* **2009**, *21*, 1595−1598.
(27) Klemm, D.; Kramer, F.; Moritz, S.; Lindström, T.; Ankerfors, M.; Gray, D.; Dorris, A. Nanocelluloses: A New Family of Nature-Based Materials. *Angew. Chem., Int. Ed.* **2011**, *50*, 5438−5466.
(28) Eichhorn, S. J.; Dufresne, A.; Aranguren, M.; Marcovich, N. E.; Capadona, J. R.; Rowan, S. J.; Weder, C.; Thielemans, W.; Roman, M.; Renneckar, S.; et al. Review: Current International Research into Cellulose Nanofibres and Nanocomposites. *J. Mater. Sci.* **2010**, *45*, 1−33.
(29) Fukuzumi, H.; Saito, T.; Iwata, T.; Kumamoto, Y.; Isogai, A. Transparent and High Gas Barrier Films of Cellulose Nanofibers Prepared by TEMPO-Mediated Oxidation. *Biomacromolecules* **2009**, *10*, 162−165.
(30) Huang, J.; Zhu, H.; Chen, Y.; Preston, C.; Rohrbach, K.; Cumings, J.; Hu, L. Highly Transparent and Flexible Nanopaper Transistors. *ACS Nano* **2013**, *7*, 2106−2113.
(31) Zhu, H.; Parvinian, S.; Preston, C.; Vaaland, O.; Ruan, Z.; Hu, L. Transparent Nnanopaper with Tailored Optical Properties. *Nanoscale* **2013**, *5*, 3787−3792.
(32) Fitz-Gerald, J. M.; Piqué, A.; Chrisey, D. B.; Rack, P. D.; Zeleznik, M.; Auyeung, R. C. Y.; Lakeou, S. Laser Direct Writing of Phosphor Screens for High-Definition Displays. *Appl. Phys. Lett.* **2000**, *76*, 1386−1388.
(33) Nj Heyn, A. The Elementary Fibril and Supermolecular Structure of Cellulose in Soft Wood Fiber. *J. Ultrastruct. Res.* **1969**, *26*, 52−68.
(34) Frey-Wyssling, A. The Fine Structure of Cellulose Microfibrils. *Science* **1954**, *119*, 80−82.
(35) Manley, R. S. J. Fine Structure of Native Cellulose Microfibrils. *Nature* **1964**, *204*, 1155−1157.
(36) Jang, J. Displays Develop a New Flexibility. *Mater. Today* **2006**, *9*, 46−52.
(37) MacDonald, W. A. Engineered Films for Display Technologies. *J. Mater. Chem.* **2004**, *14*, 4−10.
(38) Choi, M. C.; Kim, Y.; Ha, C. S. Polymers for Flexible Displays, From Material Selection to Device Applications. *Prog. Polym. Sci.* **2008**, *33*, 581−630.
(39) Hu, L.; Zheng, G.; Yao, J.; Liu, N.; Weil, B. D.; Cui, Y.; Eskilsson, M.; Karabulut, E.; Wagberg, L.; Ruan, Z.; et al. Transparent and Conductive Paper From Nanocellulose Fibers. *Energy Environ. Sci.* **2013**, *6*, 513−518.
(40) Iwamoto, S.; Kai, W. H.; Isogai, A.; Iwata, T. Elastic Modulus of Single Cellulose Microfibrils from Tunicate Measured by Atomic Force Microscopy. *Biomacromolecules* **2009**, *10*, 2571−2576.
(41) Kulachenko, A.; Denoyelle, T.; Galland, S.; Lindstrom, S. B. Elastic Properties of Cellulose Nanopaper. *Cellulose* **2012**, *19*, 793−807.
(42) Swatloski, R. P.; Spear, S. K.; Holbrey, J. D.; Rogers, R. D. Dissolution of Cellose with Ionic Liquids. *J. Am. Chem. Soc.* **2002**, *124*, 4974−4975.
(43) Fukaya, Y.; Hayashi, K.; Wada, M.; Ohno, H. Cellulose Dissolution with Polar Ionic Liquids under Mild Conditions, Required Factors for Anions. *Green Chem.* **2008**, *10*, 44−46.
(44) Liu, D.; Xia, K.; Cai, W.; Yang, R.; Wang, L.; Wang, B. Investigations About Dissolution of Cellulose in the 1-Allyl-3-Alkylimidazolium Chloride Ionic Liquids. *Carbohydr. Polym.* **2012**, *87*, 1058−1064.
(45) Fang, Z.; Zhu, H.; Li, Y.; Liu, Z.; Dai, J.; Preston, C.; Garner, S.; Cimo, P.; Chai, X.; Chen, G.; Hu, L. Light Management in Flexible Glass by Wood Cellulose Coating. *Sci. Rep.* **2014**, *4*, 5842.
(46) Fang, Z.; Zhu, H.; Preston, C.; Han, X.; Li, Y.; Lee, S.; Chai, X.; Chen, G.; Hu, L. Highly Transparent and Writable Wood All-Cellulose Hybrid Nanostructured Paper. *J. Mater. Chem. C* **2013**, *1*, 6191−6197.
(47) Liu, V.; Fan, S. S4, A Free Electromagnetic Solver for Layered Periodic Structures. *Comput. Phys. Commun.* **2012**, *183*, 2233−2244.
(48) Saito, T.; Isogai, A. TEMPO-Mediated Oxidation of Native Cellulose. The Effect of Oxidation Conditions on Chemical and Crystal Structures of the Water-Insoluble Fractions. *Biomacromolecules* **2004**, *5*, 1983−1989.
(49) Saito, T.; Nishiyama, Y.; Putaux, J.-L.; Vignon, M.; Isogai, A. Homogeneous Suspensions of Individualized Microfibrils from TEMPO-Catalyzed Oxidation of Native Cellulose. *Biomacromolecules* **2006**, *7*, 1687−1691.
(50) Saito, T.; Okita, Y.; Nge, T. T.; Sugiyama, J.; Isogai, A. TEMPO-mediated oxidation of native cellulose, Microscopic Analysis of Fibrous Fractions in the Oxidized Products. *Carbohydr. Polym.* **2006**, *65*, 435−440.
(51) Saito, T.; Kimura, S.; Nishiyama, Y.; Isogai, A. Cellulose Nanofibers Prepared by TEMPO-Mediated Oxidation of Native Cellulose. *Biomacromolecules* **2007**, *8*, 2485−2491.
(52) Isogai, A.; Saito, T.; Fukuzumi, H. TEMPO-oxidized Cellulose Nanofibers. *Nanoscale* **2011**, *3*, 71−85.

DOI: 10.1021/acsnano.5b06781
ACS Nano 2016, 10, 1369−1377